2017-24-0023

A Flow and Loading Coefficient-based Compressor Map Interpolation Technique for Improved Accuracy of Turbocharged Engine Simulations

Author, co-author (Do NOT enter this information. It will be pulled from participant tab in MyTechZone)

Affiliation (Do NOT enter this information. It will be pulled from participant tab in MyTechZone)

Abstract

Internal combustion engines are routinely developed using 1D engine simulation tools. A well-known limitation is the accuracy of the turbocharger compressor and turbine sub-models, which rely on hot gas bench-measured maps to characterize performance. Such discrete map data is inherently too sparse to be used directly in simulation, and so a preprocessing algorithm interpolates and extrapolates the data to generate a wider, more densely populated map. Methods used for compressor map interpolation vary. They may be mathematical or physical in nature, but there is no unified approach, except that they typically operate on input map data in SAE format. For decades it has been common practice for turbocharger suppliers to share performance data with engine OEMs in this form. This paper describes a compressor map interpolation technique based on the nondimensional compressor flow and loading coefficients, instead of SAE-format data. It compares the difference in compressor operating point prediction accuracy when using this method against the standard approach employing dimensional parameters. This is done by removing a speed line from a dataset, interpolating for the removed speed using the two methods, and comparing their accuracy to the original data. Three maps corresponding to compressor diameters of 54, 88, and 108 mm were evaluated. In some cases, the residual sum of squares between the interpolated and original data demonstrated an order of magnitude improvement when using the nondimensional coefficients. When evaluated in a simple engine model, this manifests as a slight shift in interpolated turbocharger speed, resulting in a difference in predicted compressor efficiency of up to 0.89 percentage points. This paper shows how the use of truly nondimensional interpolation techniques can improve the accuracy of processed turbocharger compressor maps, and consequently the value of 1D engine simulations as a reliable performance development tool, at virtually no additional effort or cost.

Introduction

Virtual product engineering has become a crucial tool in the automotive sector because it enables cost-effective development while meeting increasing levels of product complexity with ever growing validation and certification requirements. It is no longer feasible to meet increasingly compressed product development cycle durations with physical testing – a virtual test environment becomes essential. Indeed, the Automotive Council UK has set a 70% virtual validation target for 2025 [1].

Regarding virtual development of the internal combustion engine, 1D engine cycle simulation tools, both commercial (e.g., GT-POWER, Ricardo WAVE, AVL BOOST) and proprietary, have been employed over many years for purposes including performance and emissions development, engine cooling simulations, and engine-turbocharger matching. Modelling of turbocharger components in particular relies on performance ‘maps’, provided by the turbocharger supplier and measured experimentally on a hot gas bench. The resulting data is presented and shared in the form of flow and efficiency characteristics, according to a certain test procedure and reporting format, e.g., [2–4]. This specifies the use of pseudo-nondimensional parameters that enable comparison of performance measured under different laboratory conditions, and which are a compounded form of the physically-measured quantities (described later).

Turbocharger compressor maps typically comprise between 4–10 speed lines along which a finite number of data points are recorded; efficiency contours may then be overlaid, as shown in Figure 1. This discrete input data is unsuitable for direct use in simulation, and so a map preprocessing algorithm is used to interpolate and extrapolate the data to obtain a map of sufficient width and resolution.

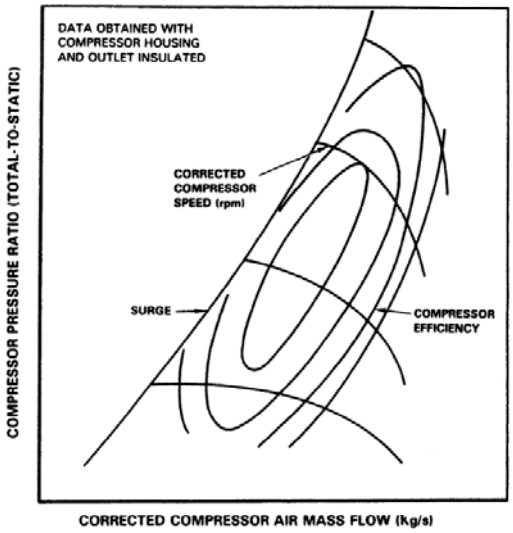

Figure 1. Typical turbocharger compressor performance map [2].

Despite the aforementioned turbocharger map measurement and data presentation standards, there is no unified method for compressor map preprocessing. Some algorithms process the corrected map,

while others process reduced or nondimensional forms of the map. There is no consensus on the preferred approach, perhaps because there is a lack of awareness that they can give different results, to a greater or lesser extent.

This issue is explored herein by comparing the map preprocessing accuracy that results from choosing a particular format of compressor performance parameters. This paper considers two options: (i) the well-known format outlined in SAE standards [2,3] that uses corrected forms of the measured *physical* quantities, and (ii) a form based on truly *nondimensional* parameters. These are referred to throughout this paper as the *physical* and *nondimensional* formats, respectively. Furthermore, the scope of this paper is purposely limited to compressor map interpolation, since extrapolation would involve making assumptions about how the map behaves outside the normal compressor operating range (and there is no unified approach for compressor map extrapolation either). Some compressor map measurements do go to very low mass flows to characterize the compressor performance in the stall region [5–7].

Once the impact of the different formats on interpolated compressor operation has been established at the component level, the corresponding compressor maps are employed in a simple engine cycle calculation to demonstrate the effect of interpolation accuracy on engine performance prediction.

Methodology

In order to assess the effect of interpolation accuracy across a range of compressor size, three publicly available [8] centrifugal compressor maps were evaluated, corresponding to impeller diameters of 54, 88, and 108 mm[1] (referred to as Maps 1, 2 and 3, respectively). For comparison, these are shown on the same axes in Figure 2.

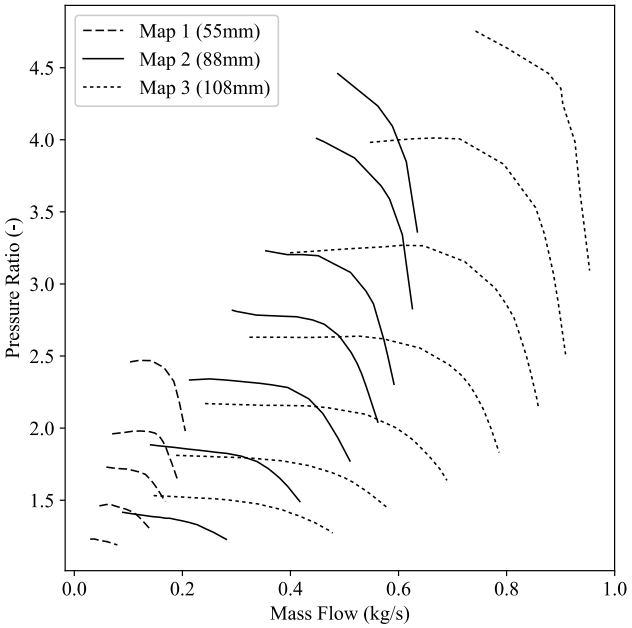

Figure 2. Pressure ratio vs. mass flow for the three subject compressors.

[1] The respective compressor models are *GT2554R*, *GTX4088R*, and *GTX5008R*.

For each map, interpolation accuracy is tested by removing a speed line and then interpolating for it, using the remaining data. The interpolated points can then be compared to the original measured points. This was carried out for all intermediate speed lines on both the physical and nondimensional map formats.

Reduction vs Nondimensionalization

Before the mathematical aspects of the preprocessing algorithm are discussed, the reader is reminded of the logic behind map reduction and nondimensionalization. Turbocharger compressor maps are measured on hot gas stands where pressures, temperatures, air flow rate and shaft rotational speed are all recorded. These are the physical quantities that can be measured directly and are easy to understand and visualize. Although these do provide a valid indication of performance, a map based just on directly-measured quantities is only useful as a means of comparison if all other compressors can be measured on the same hot gas stand under the same test conditions. Hence it is normal to apply corrections to the measured physical quantities to account for different test conditions, and so that the resulting performance maps may be used in engine cycle simulation tools.

Rotational speed is important for characterising compressor flow, but the blade tip Mach number, M_{t0}, is a more representative performance parameter since it accounts for compressibility effects:

$$M_{t0} = \frac{U}{a_0} = \frac{\left(N.\frac{30}{\pi}.\frac{D_2}{2}\right)}{\sqrt{\gamma R T_0}} \quad (1)$$

The conversion from rotational speed to tip Mach number employs the total inlet temperature T_0, as well as some fluid properties and geometric constants. For the same machine, the geometry is constant and γ and R will not change significantly, so it is convenient to define a reduced speed, N_{red}, as follows:

$$N_{red} = \frac{N}{\sqrt{T_0}} \quad (2)$$

Quantities such as the reduced speed are sometimes called quasi-nondimensional, since they are derived from a truly nondimensional parameter but ignore constants, so they do have dimensions. An alternative way of taking the inlet temperature into account for the effective compressor speed is by using a *corrected* (or *referred*) speed, which employs a temperature correction factor θ, which requires a reference temperature [9].

$$N_{corr} = \frac{N}{\sqrt{\theta}} = N\sqrt{\frac{T_{ref}}{T_0}} \quad (3)$$

The benefit of using corrected speed instead of the reduced speed is that the units and order of magnitude will be the same as the measured physical quantity, which makes it more relatable. However, the great benefit of real nondimensionalized quantities, such as M_{t0}, is that they can be used to compare different machines.

Mass flow rate is another example of a measured quantity that, by itself, does not actually give a useful indication where a particular compressor is operating with respect to the flow range of which it is capable, or against other compressors. A more indicative parameter is

the relative velocity between the flow and the blades. Since the mass flow rate is constant across a stage (the mass flow being associated with the meridional velocity), it is customary to define a *flow coefficient* ϕ, as follows:

$$\phi = \frac{C_x}{U} = \frac{\dot{m}}{\rho A_c U} = \frac{\dot{m} R T}{P A_c U} \tag{4}$$

The flow coefficient is nondimensional and thus comparable across machines. An alternative dimensionless mass flow rate is the ratio of the mass flow to the choked mass flow. This is defined as [10]:

$$\frac{\dot{m}}{\dot{m}^*} = \frac{\dot{m}}{P_0 A} \sqrt{\frac{R T_0}{\gamma}} \tag{5}$$

A reduced format of this ratio drops the terms that are the same for a given machine and constant fluid properties, i.e.,

$$\dot{m}_{red} = \frac{\dot{m} \sqrt{T_0}}{P_0} \tag{6}$$

A corrected (or referred) mass flow rate can then be created by introducing reference quantities:

$$\dot{m}_{corr} = \dot{m} \frac{\sqrt{\theta}}{\delta} = \dot{m} \sqrt{\frac{T}{T_{ref}}} \left(\frac{P_{ref}}{P} \right) \tag{7}$$

This corrected compressor air mass flow is indeed the version employed in the SAE gas stand test code [2], with T_{ref} = 298 K and P_{ref} = 100 kPa.

The remaining component of a compressor map is pressure ratio. Although inherently dimensionless, it cannot immediately be compared between different machines. An alternative parameter is the *loading coefficient*, Ψ, given by Equation (8) [10], which can be used to compare between different machines because it takes the tip Mach number into account. The term *dynamically scaled* is sometimes used to distinguish between properties that simply have no units and others that are scaled by the relevant physics [10]. The loading coefficient is a dynamically scaled pressure ratio.

$$\Psi = \frac{\Delta P}{\rho U^2} = \frac{\Pi^{\frac{\gamma-1}{\gamma}} - 1}{(\gamma - 1) M_{t0}^2} \tag{8}$$

When converting a compressor map from physical $(\dot{m}_{corr}, \Pi)$ to nondimensional (ϕ, Ψ) form, the speed lines tend to converge to a single line [11]. This can be thought of as two separate processes: alignment along the abscissa achieved by nondimensionalization of the flow parameter (most crucially dividing the flow by the speed), and alignment along the ordinate, achieved by reduction of the pressure ratio (most importantly dividing the pressure ratio by the square of the speed).

The loading coefficient for a given flow coefficient is a weak function of speed [10]. From Equation (8), this means that the pressure ratio for a given mass flow seems to be approximately a function of the square of the blade tip speed (or rotational speed).

The reduced format of the map is simply the physical map scaled by a constant, and thus there is limited benefit to studying this form. As previously mentioned, this paper focuses on comparing the physical and nondimensional map forms. These are shown for the first considered compressor map (Map 2), in Figure 3 and Figure 4, respectively.

Convergence of speed lines can be noticed in the nondimensional version of Map 2 in Figure 4, with the intermediate speed lines lying in a relatively narrow band and only the lowest and highest speed lines deviating from this. This was observed in all three maps.

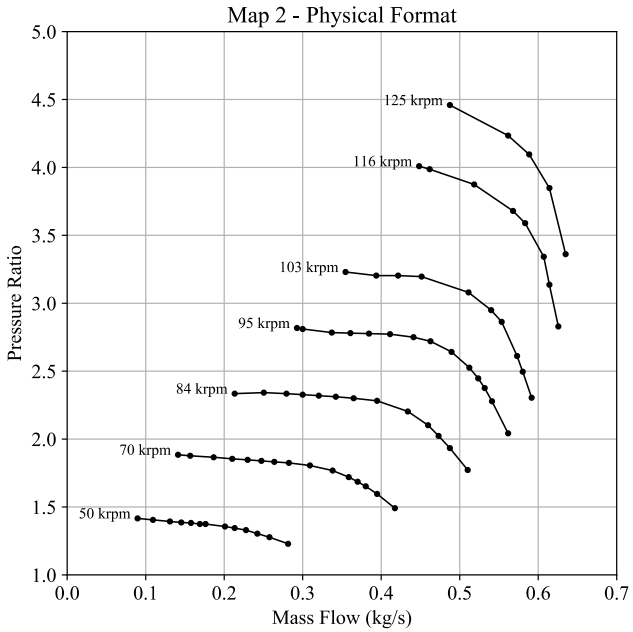

Figure 3. Physical form of Map 2.

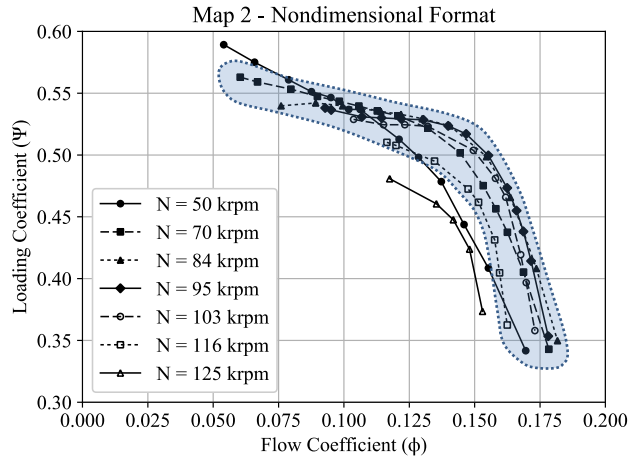

Figure 4. Nondimensional form of Map 2 highlighting the convergence of speed lines into a narrow band.

Table 1. Summary of compressor map parameters.

Map form	x (Flow)	y (Work)	z (Speed)
Physical	$\dot{m}$	Π	N
Nondimensional	ϕ	Ψ	M_{t0}

Interpolation Accuracy

Labelling the different flow parameters as the x dimension, different work parameters as the y dimension, and different measures of speed as the z dimension, then the physical and nondimensional map representations may be summarized as shown in Table 1.

Consider a scenario involving two known data points, where the objective is to find the y-value associated with any particular x-value in between. Such a scenario is shown in Figure 5, where the broken line shows the real (but unknown) relationship $y(x)$, and the solid line a linear interpolation between the given data. The purpose of Figure 5 is simply to illustrate that linearly interpolating will incur an error, the magnitude of which will depend on (i) how near the interpolated point lies to real data, and (ii) how much the real relationship deviates from linear.

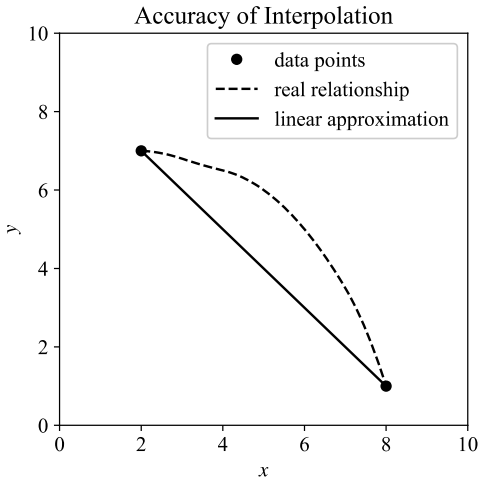

Figure 5. Error incurred by linear interpolation.

This can be extended and applied to compressor maps by considering a function $y(x,z)$, which represents an unknown relationship between compressor work and flow across different speed lines (recall from Table 1 that z is a speed parameter).

Consider two mapped dimensions (u,v), where u is the dimension along a speed line, and v is the dimension between speed lines. Definition of the latter was chosen such that v lines connect points equidistant along speed lines, though a more physically-meaningful definition such as lines of constant flow coefficient could equally be defined. The flow coefficient is a measure of the incidence angle, which is an important controlling factor in the performance of the compressor stage. This would make the v dimension simply the loading coefficient (ordinate) dimension in the nondimensional map. This approach was not taken because the speed lines do not span across the same range of flow coefficient, so extrapolation becomes necessary.

It will be seen later that a determining factor for interpolation accuracy based on the two different map formats is the linearity of the function $y(x,z)$ in the v dimension. There is also a question as to how the function behaves along the u dimension, but the methodology adopted in this paper cannot address it. Data across a given speed line is scaled by a constant, so interpolation accuracy is unaffected. Regarding alignment in x achieved by using reduced or nondimensional mass flow, it might have an influence, but it is difficult to isolate.

Mapping Algorithm

This section discusses the mapping algorithm used throughout this paper, which is robust and can accommodate various shapes of compressor map. It provides a fair way to apply an identical mapping method to the different map formats. This is important since the distribution of speeds lines differs significantly between formats.

Auxiliary coordinates are often employed to assist compressor map data handling [12]. One common way of treating compressor maps is to introduce beta-lines [9,12–14], which span the map, roughly parallel to the surge line on one side and the choke line on the other. An important drawback is that data will either need to be truncated from some speed lines, or extrapolated in others, although some works have improved the implementation of beta-lines, e.g., [13]. This study focuses on the consequences for interpolation of different map formats, so extrapolation was excluded. An alternative method, which has also been used in literature in some variations, is presented here. The method adopted is discussed in detail to give an idea of the tool. It is stressed that the authors are not claiming the mathematical mapping method to be superior to ones already available, but rather explaining it thoroughly to justify its use when comparing the physical and nondimensional map formats. Recalling that u refers to the dimension along a speed line, and v to the dimension between speed lines, the mapping algorithm steps, for a given data set, are:

1. Create fits along the u dimension. The maps used had smooth data so an exact cubic spline fit was used.
2. Sample a certain number of points along each speed line that are equally spaced in u.
3. Define lines of v by connecting corresponding points in u. A map at this stage is shown in Figure 6.
4. Create a spline fit of z against x, y along a v line.
5. Sample values of z and compute the corresponding speed lines by finding the x, y values for every v line, and connect these points along u to create the speed line.

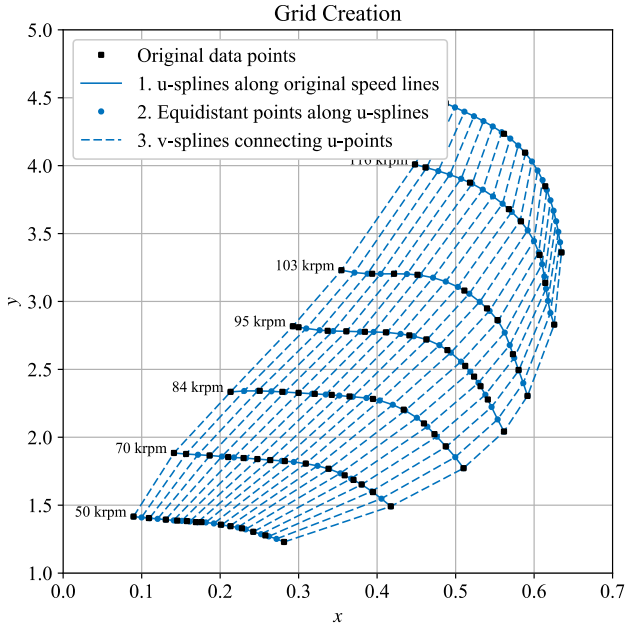

Figure 7. Grid creation process (up to step 3).

Figure 6 shows the map after step 3 is complete. The numbering in the legend corresponds to the numbering of the steps.

As mentioned in step 1, the fit to the speed lines was a spline, which provided an exact fit. The data used for this study was supplier data that had already been smoothed. Therefore, a least-squares fit was not required. However, if the data is not smooth, this step could be done with an appropriate curve fit. Polynomials have shown poor performance in previous works, but an ellipse fit to the speed lines showed good accuracy [15,16] and could be employed. The spline along v (henceforward referred to as the *v* line) was initially tested with a linear spline. (Additional tests using a quadratic spline were also performed, and will be explained in the next section.) For the linear spline, the spacing of the sampled speed lines between two original speed lines is independent of the other original speed lines.

The mapping algorithm creates a grid across the entire map. The grid density is controlled by the number of sampled points along u, v. For all work described in this paper, the grid was chosen to be fine enough such that results are grid-independent. The described method will be familiar to many applications in the field (and many other fields such as graphical representations and meshing). The only additional assumption imposed to this established method is the assignment of the speed value to the sampled speed lines. One would tend to abide by simplicity and linearly space the speed lines. The plots of nondimensionalized maps suggest a square relationship, but this would not be conducive when assigning a speed value for the sampled speed lines.

Interpolation Technique & Test Method

With the grid created, the interpolation technique for finding y given x, z can be described:

1. Find the two speed lines between which z lies, and λ, the fractal distance from the first speed line.
2. Evaluate y_1, y_2 as the values of y given by the two speed lines.
3. Linearly interpolate between y_1, y_2 using λ.

With a robust mapping algorithm described, the testing methodology can now be introduced, the aim of which is to quantify the predictive capability of the mapping algorithm. The steps followed are:

1. Redefine the original data set by removing a speed line (and its associated data).
2. Run the mapping algorithm on the new data set.
3. Use the new grid and its associated interpolation algorithm to interpolate for the missing speed line.
4. Compare the interpolated data to the original data.
5. Repeat steps 1-4 for all the intermediate speed lines.

This test can only be applied on intermediate speed lines (i.e., those lying between the lowest and highest speed lines), since extrapolation was deemed out of scope.

The quality of interpolation is calculated using the residual sum of squares, $SS_{\text{res},i}$, such that:

$$SS_{\text{res},i} = \sum_j \left(f(x_j) - y_j\right)^2 \tag{9}$$

In this notation, index i refers to the v dimension (speed line number) and j to the u dimension (along a speed line). Clearly, a smaller residual sum is better, since it signifies less error between the predicted values and the original data points. A residual sum of 0 would mean a perfect fit (at the tested points). An alternative measure is the coefficient of determination, or R^2 value, such that:

$$R_i^2 = 1 - \frac{SS_{\text{res},i}}{SS_{\text{tot},i}} \tag{10}$$

where:

$$SS_{\text{tot},i} = \sum_j \left(\bar{y} - y_j\right)^2 \tag{11}$$

This compares the predictive capability of the fit to using the mean value of that data (per speed line, in this case), where $R^2 = 1$ indicates a perfect fit, and a negative R^2 suggests that a mean value predicts the required values better than the fit.

An overall performance evaluation can be obtained if the residual sum of squares of all speed lines is added. This gives a parameter that can be used to compare different interpolation methods on the same map, but not between different maps. The parameter will be referred to as SSS_{res}, the sum of residual sum of squares.

$$SSS_{\text{res}} = \sum_i SS_{\text{tot},i} \tag{12}$$

Note that SSS_{res} will be calculated on the physical map. The reduced and nondimensional data will be converted to physical before the comparison to the original data.

Another comparison parameter is the *MRE*, the mean of the relative errors across the map, where the relative error, *RE*, for each point is:

$$RE_j = \left|\frac{f(x_j) - y_j}{y_j}\right| \tag{13}$$

Results & Discussion

An example grid is displayed in Figure 7, showing example *u*- and *v*-lines. The grid density used in calculations is much higher than shown in the figure. It was reduced to make the figure clearer, but later increased to ensure the solution is grid-independent. Grids generated for the physical and nondimensional maps are somewhat similar, but since the speed lines are closer together it is more difficult to see the grid results.

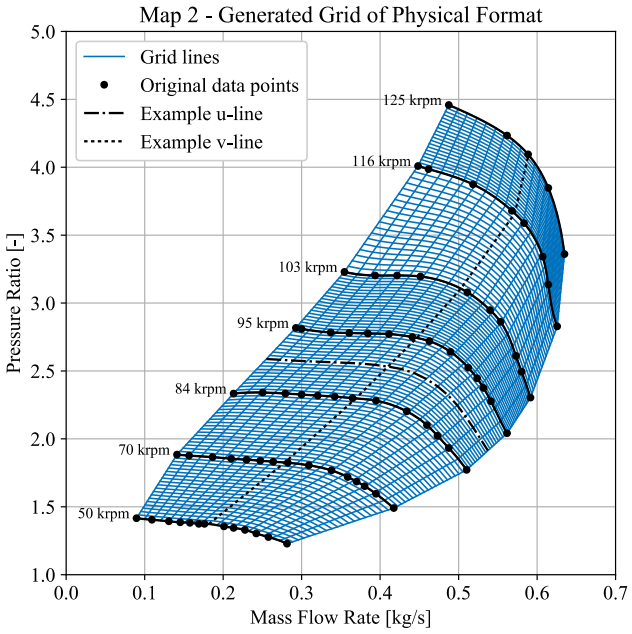

Figure 8. Grid generated for the physical map format (Map 2).

The speed line removal iterations are run and the resulting maps are created. An example of the physical map with the third speed line (95 krpm) removed is given in Figure 8, for Map 2 (88 mm impeller).

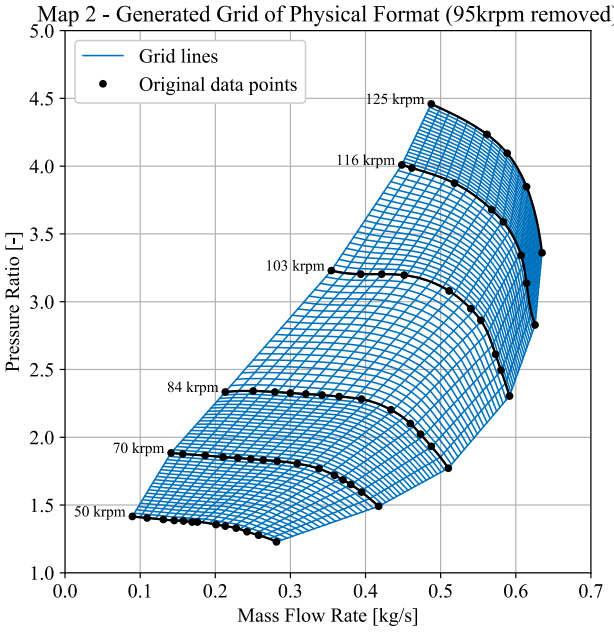

Figure 9. Physical map grid with 95 krpm speed line removed.

The new maps with removed speed lines are used to interpolate for their respective missing speed lines. This is done separately on the physical and nondimensional maps. The interpolation is done on x values corresponding to the original data points on the removed speed lines. The resultant points are created in the same parameter format as the map they were interpolated from, but then results from the nondimensional maps are re-dimensionalized so that they can be plotted on the physical maps for comparison. When a speed line is removed, however, the grid generated from the adjacent speed lines will not always encapsulate the removed line, i.e., its first and last points may lie outside of the grid. This shifting effect on grid boundaries can be seen in Figure 9 for five different data subsets.

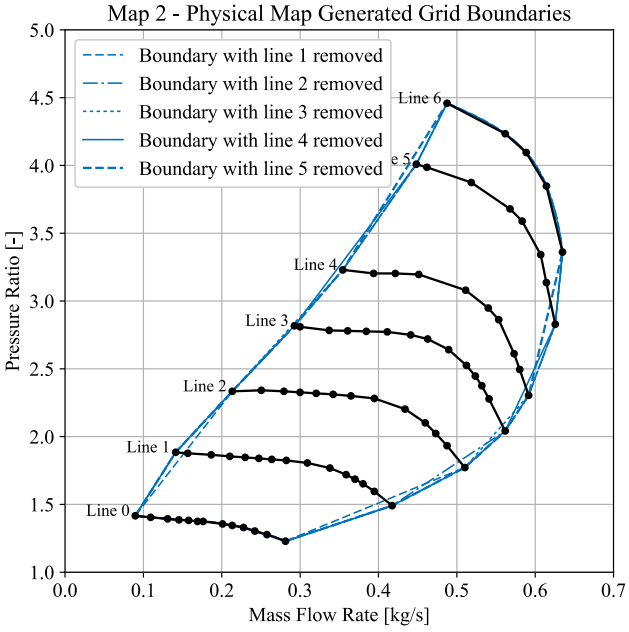

Figure 10. Changing grid boundaries as speed lines are removed.

Taking *Line 1* in in Figure 9 for example, the broken blue line represents the bounds of the grid generated when *Line 1* is removed, but the end data points of *Line 1* lie outside of this region. Any such outlying points were not evaluated, to avoid extrapolation, but to ensure a consistent approach the end points of *all* speed lines were excluded from interpolation testing.

The resulting interpolated points from the two different map formats, all converted into dimensional form, are plotted in Figure 10 along with the original data. It can be seen that the nondimensional-based interpolation is far superior to that based on the physical map at the lower two speed lines. From the analysis of the data it seems that at least for the lower values of M_{t0} (i.e., lower rotational speeds), $\Psi(\phi, M_{t0}) \sim N^0$. The speed lines are closely stacked, and the loading coefficient varies little in that regime. This means that $\Pi(\dot{m}, N) \sim N^2$. The fact that Ψ is a weak function of speed seems to greatly improve interpolation accuracy in the v dimension. The advantage afforded by the nondimensional-based interpolation is however not so clear at the higher speed lines. This is likely related to the aforementioned phenomenon that speed lines start to diverge from a single stack at high speed.

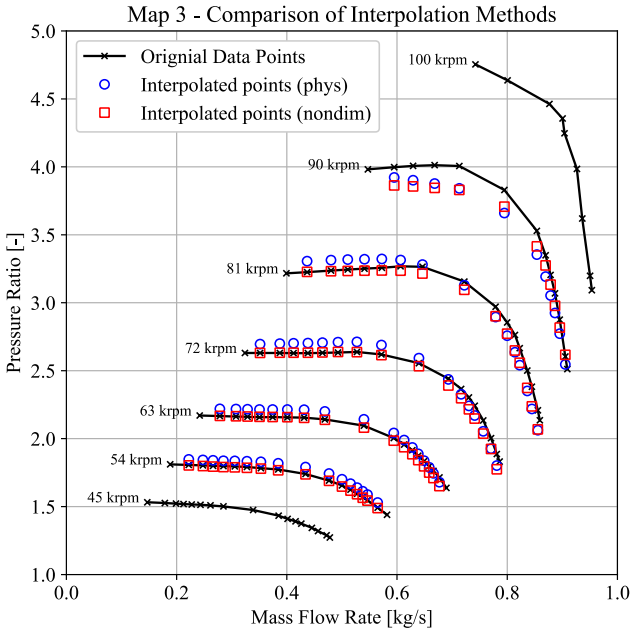

Figure 11. Interpolation comparison (Map 2).

As previously mentioned, standard fitting parameters such as the residual sum of squares and the coefficient of determination are used to evaluate the accuracy of the interpolation. The sum of residual sums of squares (SSS_{res}) and the mean relative error (*MRE*) were calculated as a measure of the overall accuracy of interpolation across the entire map. The resulting numbers, shown in Table 2, support the observations in Figure 10.

Table 2. SSS_{res} and *MRE* (in parentheses) for all maps.

Map	Map 1	Map 2	Map 3
D_2 (mm)	54	88	108
Physical SSS_{res} (*MRE*)	0.488 (0.56%)	0.254 (1.3%)	0.048 (0.95%)
Nondim. SSS_{res} (*MRE*)	0.318 (0.36%)	0.126 (0.88%)	0.038 (0.67%)

Figure 10 shows the nondimensional map is better than the physical format at predicting lower speed values. In fact, for the 70 krpm line, the coefficient of determination for the physical map is negative. As previously described, this means that the speed line would have been better predicted based on the mean pressure ratio value than by using the interpolation functions. While that speed line is particularly flat, exacerbating this aspect, it is surprising that the physical maps perform so poorly in this regard. Based on the SSS_{res} and *MRE*, interpolation based on the nondimensional map provides a significant improvement over the physical map, for all three compressor sizes.

Similar trends of noticeably superior performance at the lower speeds are seen in all cases. To help illustrate this, the interpolation results of Map 3 are plotted in Figure 11.

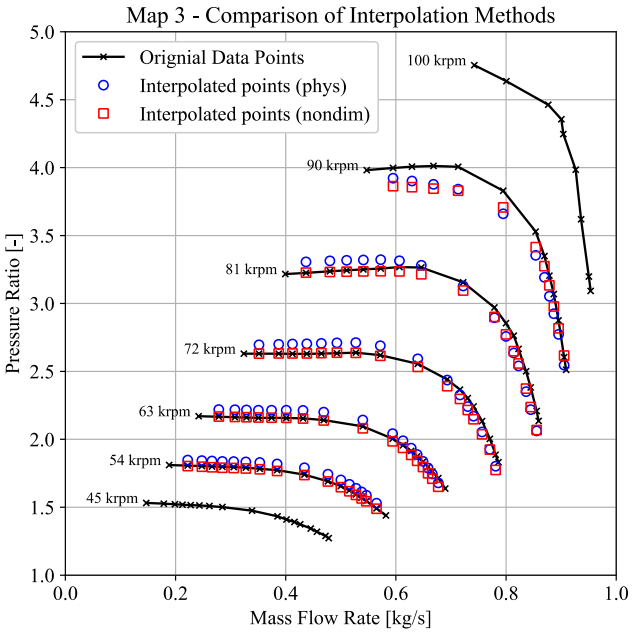

Figure 12. Interpolation comparison (Map 3).

It can be seen from Figure 10 and Figure 11 that at low speeds, the physical map predicts speed lines that lie above the original data in their entirety. The linear spline used to sample the speed lines essentially places them equidistantly between the surrounding speed lines. The spacing of the speed lines is thus a function of its two neighbouring lines.

There is no physical reason why this should be so. Hence it was decided to perform another set of tests where placement of speed lines takes into account the general speed trend across the map, by switching the order of the *v*-line from linear ($\mathcal{O}1$) to quadratic ($\mathcal{O}2$), to improve the accuracy of the interpolation method. An example grid with quadratic splines is shown in Figure 12. Indeed, using a non-linear fit between speed lines is more representative of modern-day mapping tools.

An example plot of interpolation results using the quadratic grid is shown in Figure 13. It is immediately seen that there is a large benefit from switching from a linear spline to a quadratic spline. The benefit varies between maps. Map 1 shows an order of magnitude improvement when increasing the order of the *v*-line, whereas for Map 2 the improvement is on average less than 50% (which is still very significant, of course).

If a better placement of speed lines is the main advantage of the nondimensional map, the SSS_{res} of the nondimensional method should not see as drastic an improvement as the physical map when using the quadratic grid, but Figure 13 still shows a further useful improvement in accuracy.

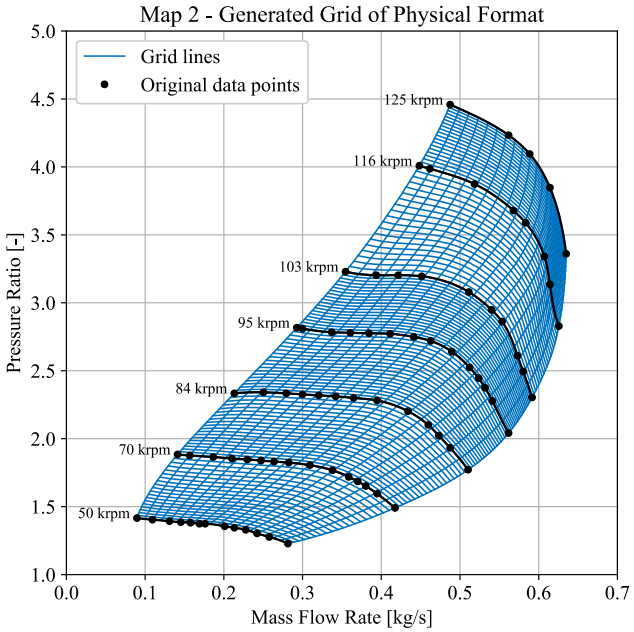

Figure 13. Example quadratic spline grid.

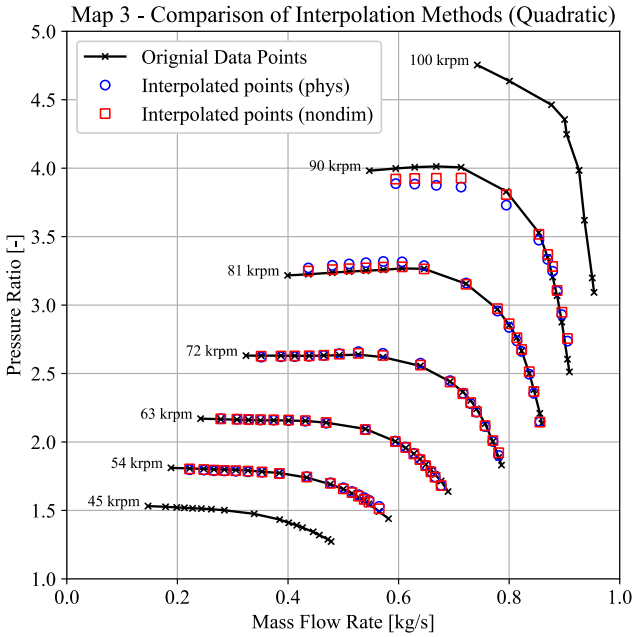

Figure 14. Comparison of quadratic spline interpolation (Map 3).

A full list of the SSE_{res} and MRE values derived from the two map formats using linear and quadratic splines, and for each of the three compressor sizes, is given in Table 3. The dimension given in parentheses is the compressor outer diameter (D_2), which is used in nondimensionalization. The ranking of interpolation accuracy in Maps 2 and 3 is the same as Map 1: interpolation using the nondimensional map is clearly an improvement over that using the physical map. These results suggest that reducing the data improves

interpolation accuracy using the current mapping method. The nondimensionalization provides a 30–33% relative improvement in the *MRE*.

Table 3. Comparison of first and second order *v*-line interpolation.

Map	Map 1	Map 2	Map 3
$\boldsymbol{D_2}$ $(\boldsymbol{mm})$	54	88	108
Physical $O1$ SSS_{res} (*MRE*)	0.488 (2.7%)	0.254 (2.0%)	0.048 (2.8%)
Physical $O2$ SSS_{res} (*MRE*)	0.137 (0.56%)	0.016 (1.3%)	0.029 (0.95%)
Nondim. $O1$ SSS_{res} (*MRE*)	0.318 (1.2%)	0.126 (1.2%)	0.038 (1.6%)
Nondim. $O2$ SSS_{res} (*MRE*)	0.076 (0.36%)	0.008 (0.88%)	0.015 (0.67%)

The nondimensional map still maintains a strong advantage in accuracy over the physical map, and actually seems to benefit more from the upgrade to quadratic splines. The lower speed lines on the physical map are also predicted much more accurately with the quadratic spline method. Both methods perform worse at the highest speed lines, especially at higher mass flows close to choke, where the gradients are very steep.

The normalized work and flow as functions of speed along *v*-lines are investigated in order to better understand why the nondimensional map benefits more from the higher order splines. The deviation of the speed changes between linear and quadratic can be seen in Figure 14. The coordinates are normalized speed *zn*, against normalized flow and work xn, yn for the physical form of Map 1. To clarify, the normalization is carried out such that the entire normalized range *tn* of a variable *t* lies between 0 and 1, as per Equation (14).

$$tn = \frac{(t - t_{\min})}{t_{\max} - t_{\min}} \qquad (14)$$

Figure 14 shows selected *v*-lines, from the surge line to choke. To clarify, the lines in Figure 14 are normalized flow and work as a function of normalized speed along *v*-lines, like the one shown in Figure 7. The lowest line in the normalized flow plot will be that closest to surge, while the uppermost line is closest to choke. This order is reversed in the normalized work plot. The difference between the linear and quadratic spline traces shows the benefit of upgrading the spline order in capturing the curvature. Figure 15 shows Map 1 nondimensional speed variations. Clearly, there is a large benefit here of using the quadratic splines over the linear. This benefit is exacerbated when a speed line is removed. The benefit is shown statistically by the significant improvement of the SSS_{res} of nondimensional Map 1 between first and second order splines, as listed in Table 3. This particular map was chosen because it showed a much larger improvement when increasing the spline order in the nondimensional format than the physical format. In fact, there is always a benefit moving from linear to quadratic, but that benefit is stronger for the case of the nondimensional format. Figure 14 and Figure 15 show that this is due to the higher curvature in the nondimensional format that is better captured using a higher order spline.

The higher speed lines show a large interpolation error in all cases. It was seen earlier that in this area the speed lines deviate from the single stack in the nondimensional format (Figure 4). It seems that the map is changing in a way that is inadequately captured by the curve fits to the input data.

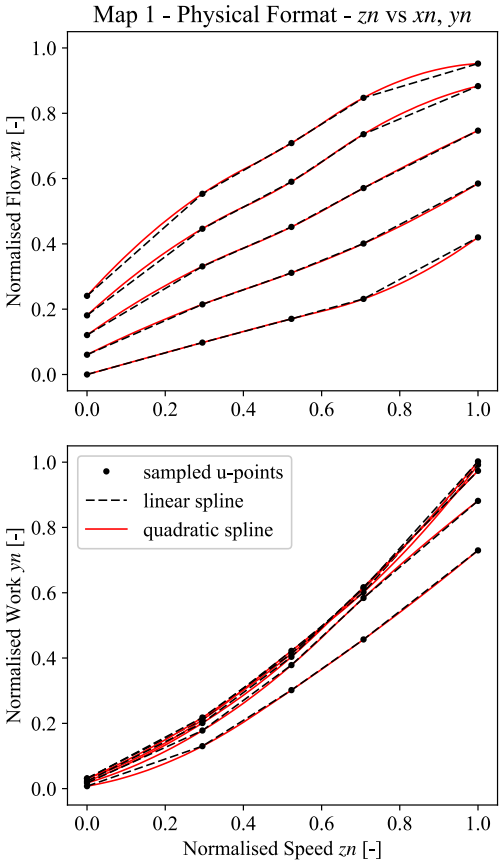

Figure 15. Speed variations in *x,y* (Map 1, physical).

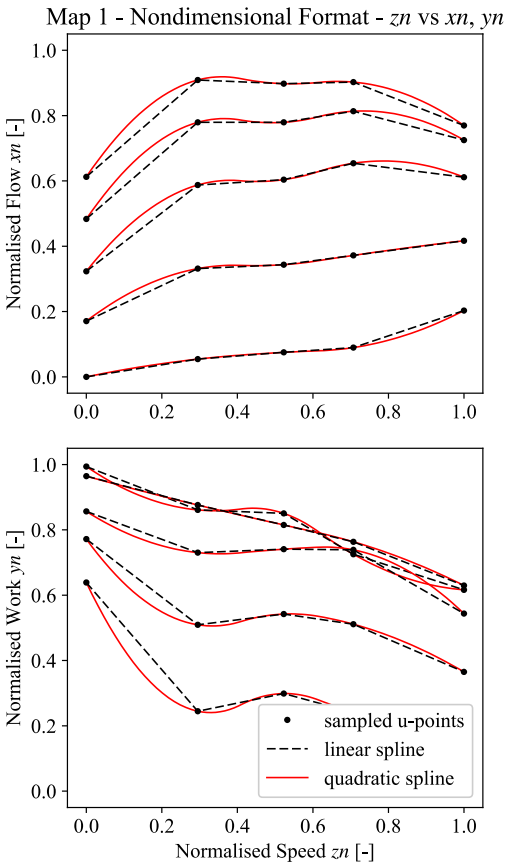

Figure 16. Speed variation in x,y (Map 1, nondimensional).

Impact on Predicted Engine Performance

This section aims to qualify the work by briefly assessing how the choice of compressor map format and the resulting interpolation accuracy is translated to the system level, in terms of predicted engine performance parameters.

A simple SI gas cycle engine model found in [17] is used for this evaluation. The model is set up for a single-stage turbocharged 1.8L PFI gasoline engine (with stoichiometric fueling). Turbocharger operation is derived from compressor and turbines maps, but constant turbine efficiency is purposely assumed so as not to obscure the effect of compressor map interpolation at the engine level.

The required compressor operating point is determined by the engine speed and target power. This is in the form of the required boost (converted to pressure ratio by employing the inlet pressure) and the physical mass flow rate. The combination of flow rate and pressure ratio is converted by the map to a speed. The method to evaluate the speed is similar to that used in [18]. With the speed and mass flow known, the efficiency can be evaluated. To clarify, the efficiency was read off a physical map directly. A nondimensional form of the efficiency map was not created, mainly because the focus of this work was the flow-work map. Another reason is that it is not immediately clear what treatment the efficiency would need in order to achieve the same effect as the conversion from pressure ratio to loading coefficient (if any). It is worth mentioning that even reducing the flow in an efficiency-flow plot does cause the lines to coalesce, and the efficiency becomes a much weaker function of the speed. Such a map can be found in [19]. Investigation into the reduction of the efficiency map is a possibility for future work.

One numerical issue arose when attempting to evaluate the speed from the nondimensional map. When converting from mass flow and pressure ratio to flow and loading coefficient, the speed is required, and it is unknown. It is difficult to guess a starting value based on the nondimensional map alone, since all the lines are so close to each other. Even with a reasonable guess for initial speed, it is difficult to evaluate the tip Mach number for a flow coefficient – loading coefficient. To overcome this, a reasonable starting speed was inferred from the physical map work, and thus a window for the probable speed lines in the nondimensional domain was specified. Nevertheless, it is clear that the nondimensional map, although more accurate, is more difficult to use directly in an engine simulation.

If there is a difference between the predictions due to map format it will first appear in the compressor operating point. The different map formats will interpret the same compressor operating point on a different speed. A different speed will lead to different compressor efficiency, changing the demanded power from the turbine, thus changing the turbine expansion ratio and wastegate bypass fraction. This will have an effect on the net IMEP, and consequently the fuel consumed to meet the power requirements.

Even though the differences in the interpolated speed lines were shown to be relatively large, the same is not to be expected from the overall engine performance parameters. The interpolation inaccuracies quantified by the sum of residual sum of squares somewhat exaggerates the effect since speed lines are removed from the map, making it slightly worse at predicting values. Also, inaccuracies translate to a turbocharger speed difference, which is used to evaluate efficiency. Changes in speed are more likely to move along efficiency contours rather than across them, due to the nature of compressor maps. The change in efficiency and its consequent changes in turbine operating point affect the pumping losses, represented by the PMEP. At most engine loads, PMEP remains a relatively small fraction of net IMEP, so a fractional change in PMEP is unlikely to change net IMEP significantly.

Several different engine operating points and different compressor maps were tested. For the simulated 1.8L engine, the compressor associated with Map 1 (which has a 54 mm compressor wheel) is a good match (the other two compressors being too large). However, by utilizing simple scaling factors, data from the larger maps can be used in this study as well. Table 4 lists predicted engine performance obtained for the physical and nondimensional map interpolation techniques for a target engine power of 39 kW at an engine speed of 2900 rpm. Clearly, the engine operating parameters are not severely affected by the different interpolation methods. The differences shown are likely smaller than the error bars associated with measuring these quantities, and certainly smaller than the errors caused by the model assumptions. Some of the reasons for the small changes were already discussed. An additional reason was observed when studying the different converged points. Considering typical compressor map efficiency contours, a small change in speed for the same mass flow will usually result in a small change in efficiency, since the change path is more or less aligned with the efficiency contours. In this example there was a change of 0.6 percentage points in compressor efficiency between the two maps.

Table 4. Comparison of predicted engine performance (2900 rpm, 39 kW).

Parameter	Physical map	Nondimensional map	Difference
PMEP (bar)	0.680	0.676	0.59%
$IMEP_{net}$ (bar)	9.062	9.062	0.00%
N_c (krpm)	86.70	86.00	0.81%
η_c (%)	72.02	72.62	0.60 %-age points (or 0.83%)

Although compressor maps do not exhibit large efficiency changes due to small differences in interpolated speed, there were some extreme cases (e.g., Table 5) where the different format maps predicted 0.89 percentage points of efficiency difference. (Results in Table 5 were produced using a version of Map 3 that had been scaled, as previously mentioned.) Depending on one's point of view, this is quite significant, as an improvement even of a single point of efficiency in compressor design optimization is considered an impressive feat. For example, the volute inlet height adjustment reported in [20] achieved a ~0.4 percentage-point improvement in compressor total-to-total efficiency. Although perhaps not significant when applied to a basic engine performance calculation, turbocharger suppliers expend significant time and effort to implement a gain even of this small magnitude.

Table 5. Comparison of predicted engine performance (3000 rpm, 57.5 kW).

Parameter	Physical map	Nondimensional map	Difference
PMEP (bar)	0.368	0.374	1.41%
$IMEP_{net}$ (bar)	12.91	12.91	0.00%
N_c (krpm)	80.23	81.41	1.47%
η_c (%)	70.02	69.13	0.89 %-age points (or 1.27%)

Conclusions

Virtual engine development is an essential tool in the automotive sector, and compressor maps remain integral to the representation of turbocharger performance in engine simulations today. Maps of pressure ratio versus corrected flow for different corrected speeds are employed in many commercial and proprietary simulation tools. An alternative way to represent compressor performance is to use the flow and loading coefficients. This paper evaluated the beneficial impact on map-interpolated compressor operation by employing these nondimensional quantities.

A mathematical mapping method was developed and applied to maps pertaining to three sizes of compressor impeller diameter: 88, 108, and 54 mm (Maps 1, 2 and 3, respectively), in both physical (corrected) and nondimensional formats. The accuracy of their interpolation was tested by removing a speed line from the original data set, creating the map grid and equations, and interpolating for the missing speed lines. This was done for all intermediate speed lines on all three maps. Speed lines were created using either linear or quadratic splines in the *v* direction.

The benefit of compressor map nondimensionalization was discussed and demonstrated through interpolation testing and estimation of the compressor operating point in a simple engine cycle calculation. The choice of the method of map processing was shown to give very different results when attempting to recreate missing speed lines from the original maps. This was quantified via the sum of residual sum of squares and the mean relative error. It was shown that the nondimensional map is always superior in terms of interpolation accuracy, compared to the physical (corrected) map, and particularly at low compressor speeds. It is surmised that in this region, where the speed lines are closely stacked, $\Psi(\phi, M_{t0}) \sim N^0$, and the loading coefficient varies little, implying that $\Pi(\dot{m}, N) \sim N^2$. The fact that Ψ is a weak function of speed seems to greatly improve interpolation accuracy in the *v* dimension, and so the compressor tip Mach number was shown to be an important parameter for nondimensionlization.

Furthermore, an interpolation grid based on a quadratic spline is significantly more accurate for either approach. Generally, the spline order had a larger impact than nondimensionalization, but the extent of this varied greatly between maps. The quadratic spline improved the SSS_{res} by up to 93%, while nondimensionalization improved the SSS_{res} by up to ~50%. The mean relative error showed a relative reduction of over 30% when comparing the nondimensional to physical formats for all three maps considered. The compressor maps were then employed in a simple SI engine cycle calculation, to see the effect of map formats on the compressor operating point and engine performance parameters. A difference of up to 0.89 percentage points of compressor efficiency was seen in one case. This is a significant magnitude in the context of compressor design, although it had a minor impact at the engine level.

Overall, this work has shown that nondimensionalization of compressor map data improves interpolation accuracy using the current mapping method. The authors therefore recommend that compressor map interpolation methods for engine cycle simulation tools are better founded on the nondimensional flow and loading coefficients (if not already) than the more commonplace physical (corrected) parameters, since the former has been shown to be more accurate for predicting turbocharger compressor performance in the considered test cases.

References

1. Jackson, N., "Automotive Council The Digital Revolution – The Potential for Virtual Product Engineering in the Automotive Sector," Automotive Council UK Virtual Product Engineering Roadmap, 2016.

2. SAE International Surface Vehicle Recomended Practice, Turbocharger Gas Stand Test Code, 1995.

3. SAE International Surface Vehicle Recomended Practice, Turbocharger Nomenclature and Terminology, 1995.

4. ASME, Performance Test Code on Compressors and Exhausters PTC 10-1997, 1997.

5. Galindo, J., Serrano, J.R., Climent, H., and Tiseira, A., "Experiments and modelling of surge in small centrifugal compressor for automotive engines," *Exp. Therm. Fluid Sci.* 32(3):818–826, 2008, doi:10.1016/j.expthermflusci.2007.10.001.

6. Marelli, S., Carraro, C., Marmorato, G., Zamboni, G., and Capobianco, M., "Experimental analysis on the performance of a turbocharger compressor in the unstable operating region and close to the surge limit," *Exp. Therm. Fluid Sci.* 53:154–160, 2014, doi:10.1016/j.expthermflusci.2013.11.025.

7. Dehner, R., Selamet, A., Keller, P., and Becker, M., "Prediction of Surge in a Turbocharger Compression System vs. Measurements," *SAE Int. J. Engines* 4(2):2181–2192, 2011, doi:10.4271/2010-01-2142.

8. Garrett, "Product Catalogue," Honeywell International Inc., 2016.

9. Baines, N.C., "Fundamentals of Turbocharging," Concepts NREC, Vermont, USA, 2005.

10. Cumpsty, N.A., "Compressor Aerodynamics," Reprint Ed, Krieger Publishing Company, Malabar, Florida, 2004.

11. Fink, D.A., Cumpsty, N.A., and Greitzer, E.M., "Surge Dynamics in a Free-Spool Centrifugal Compressor System," *J. Turbomach.* 114(2):321–332, 1992, doi:10.1115/1.2929146.

12. Kurzke, J., "How to Get Component Maps for Aircraft Gas Turbine Performance Calculations," *ASME Turbo Expo Power Land, Sea Air* 5, 1996, doi:10.1115/96-GT-164.

13. Misté, G.A. and Benini, E., "Improvements in off design aeroengine performance prediction using analytic compressor map interpolation," *Int. J. Turbo Jet Engines* 29(2):69–77, 2012, doi:10.1515/tjj-2012-0012.

14. Orkisz, M. and Stawarz, S., "Modeling of turbine engine axial-flow compressor and turbine characteristics," *J. Propuls. Power* 16(2):336–339, 2000.

15. Leufvén, O. and Eriksson, L., "A surge and choke capable

compressor flow model-Validation and extrapolation capability," *Control Eng. Pract.* 21(12):1871–1883, 2013, doi:10.1016/j.conengprac.2013.07.005.

16. Eriksson, L., Nezhadali, V., and Andersson, C., "Compressor Flow Extrapolation and Library Design for the Modelica Vehicle Propulsion Library - VehProLib," *SAE Tech. Pap.*, 2016, doi:10.4271/2016-01-1037.

17. Ferguson, C.R. and Kikrpatrick, A.T., "Internal Combustion Engines," John Wiley & Sons, 2001.

18. Thomasson, A., Llamas, X., and Eriksson, L., "Turbo Speed Estimation Using Fixed-Point Iteration," *SAE Technical Paper*, 2017, doi:10.4271/2017-01-0591.

19. Fink, D.A., "Surge dynamics and unsteady flow phenomena in centrifugal compressors," PhD Thesis, Massachusetts Institute of Technology, 1988.

20. Kim, S., Park, J., Ahn, K., and Baek, J., "Improvement of the Performance of a Centrifugal Compressor by Modifying the Volute Inlet," *J. Fluids Eng.* 132(September):91101, 2010, doi:10.1115/1.4001972.

Contact Information

Dr Aaron Costall
Imperial College London
Department of Mechanical Engineering
South Kensington Campus
London SW7 2AZ
UK

Email: a.costall@imperial.ac.uk

Acknowledgement

The authors would like to thank Caterpillar Inc. for their financial support and close technical collaboration on this work.

Disclaimer

Definitions

A_c	Reference compressor flow area
C_x	Average axial velocity
D_2	Compressor wheel diameter
MRE	Mean relative error
M_{t0}	Tip Mach index
N	Compressor speed
P	Pressure
R	Gas constant
R^2	Coefficient of determination
SS_{res}	Residual sum of squares
SS_{tot}	Total sum of squares
SSS_{res}	Sum of residual sum of squares
T	Temperature
U	Blade tip speed
a_0	Isentropic speed of sound (ambient values)
$\dot{m}$	Mass flow rate
$\dot{m}^*$	Choked mass flow rate
u	Mapped dimension – parallel to speed line
v	Mapped dimensions – between speed lines
x	Flow parameter $(\dot{m}, \phi)$
y	Work parameter (Π, Ψ)
z	Speed parameter (N, M_{t0})
xn, yn, zn	Normalized parameter
Π	Pressure ratio
Ψ	Loading coefficient
γ	Ratio of specific heats
δ	Referred pressure correction factor
η	Efficiency
θ	Referred temperature correction factor
ρ	Density
ϕ	Flow coefficient

Abbreviations

IMEP	Indicated mean effective pressure
ISFC	Indicated specific fuel consumption
PMEP	Pumping mean effective pressure